

# Preparation of Ni/Mn compounds/ordered mesoporous carbon composite for use in an electrochemical supercapacitor

Jicheng Feng · Bohejin Tang · Jiachang Zhao ·  
Ping Liu · Jingli Xu

Received: 22 April 2010 / Accepted: 18 April 2011 / Published online: 30 April 2011  
© Springer Science+Business Media B.V. 2011

**Abstract** The electrochemical behavior of a series of composites synthesized by a combination of incipient wetness impregnation and hydrothermal method for the first time is systematically compared (using cyclic voltammetric and electrochemical impedance spectroscopic analyses). Structural and morphological characterizations of the composites were undertaken using power X-ray diffraction (XRD), N<sub>2</sub> adsorption/desorption isotherms and transmission electron microscopy (TEM). The results indicated that the binary nickel/manganese compounds of the Ni–Mn/ordered mesoporous carbon (OMC) composite had a synergistic effect of both components.

**Keywords** Synergistic effect · Incipient wetness impregnation · Hydrothermal · Composite

## 1 Introduction

Supercapacitors have been widely recognized as a unique electrochemical device which is designed to possess high specific energy and power density [1, 2]. However, their energy density is relatively low in comparison with that of the rechargeable batteries. These devices are generally divided into electric double-layer capacitors (EDLCs) and pseudo-capacitors based on the energy storage mechanism [3–5].

In order to increase the performance of supercapacitors, various permutations and combinations of metal compounds and other organic and inorganic moieties have been investigated [6–18]. Such materials are added either *in situ* during synthesis or mixed during the electrode preparation. Mixed metal compounds are preferred to help in augmenting the capacitances as they tend to be complementary in their properties. Considering the typical example of NiO, it is known that it has modest electrochemical properties. In combination with carbon nanotubes, its electronic and redox properties get improved so that higher electrochemical capacitances are achieved [6]. Owing to the consideration of cost and the electron/proton conductivity, RuO<sub>2</sub>-based composites, such as Multi-Walled Carbon Nanotube (MWCNT)/RuO<sub>2</sub> [7], Active Carbon Black (ACB)/RuO<sub>x</sub> [8], CMK-3 (one kind of mesoporous carbon)/RuO<sub>x</sub> [9], and mixed-oxide composites [10, 11] have been extensively studied. Other examples are Vapor Grown Carbon Fiber (VGCF)/RuO<sub>2</sub>·xH<sub>2</sub>O [12], Carbon nanotubes (CNT)/MnO<sub>2</sub> [13–16], MnO<sub>2</sub>·xH<sub>2</sub>O/Carbon Resorcinol Formaldehyde (CRF) [17], and NiO/CNT [6]. Other binary metal compounds and carbon have been reported, such as MnFe<sub>2</sub>O<sub>4</sub>/carbon black [18].

A number of currently studied electrode materials are based on the carbon materials above. These materials demonstrate significant electrochemical activity; however, the outstanding electrochemical properties and unique charge transfer channel of ordered mesoporous carbon (OMC) make them the most promising candidate for electronic applications. The present application of the OMCs only took advantage of its double-layer capacitance. It is reported that OMC can be used as the host material to prepare host–guest composite material by drawing metal compounds into its pores [19, 20].

Apart from individual compounds, the electrochemical behavior of complex compounds and hydroxides of Ni/Mn

J. Feng (✉) · B. Tang (✉) · J. Zhao · P. Liu · J. Xu (✉)  
College of Chemistry and Chemical Engineering, Shanghai University of Engineering Science, Shanghai 201620, China  
e-mail: fjc0422@163.com

J. Xu  
e-mail: xujingli@sues.edu.cn

and OMC synthesized by a combination of incipient wetness impregnation method has not been studied extensively by now. The OMCM composite obtained by the novel method demonstrated significant synergistic effect in this system. Moreover, the most interesting phenomenon is that the host material (OMC) can supply the carbon source to obtain  $\text{MnCO}_3$  from 50%  $\text{Mn}(\text{NO}_3)_2 \cdot 6\text{H}_2\text{O}$ . The focus of investigation reported here is the synthesis and characterization of a nano-scale OMCMN, OMCM, OMCN, and OMC by a combination of incipient wetness impregnation and hydrothermal method for the first time. Electrochemical characterization of the composites is undertaken by means of cyclic voltammetry to screen the effect of OMC and nickel compounds on the faradic pseudo-capacitive response of manganese compounds. The use of OMC as the best substrate material has been emphasized in recent publications by Zhu et al. [19, 20]. The electrochemical performance of OMCMN, OMCM, OMCN, and OMC is examined in 2 M KOH solution.

## 2 Experimental

### 2.1 Preparation of OMC/binary Ni–Mn compounds composite

All reagents used in this experiment were of analytic grade without further purification. Water used in the synthesis and washing was deionized. Research grade nickel foil was purchased from Shanghai metal foil plant.

SBA-15 silica was prepared using the triblock copolymer,  $\text{EO}_{20}\text{PO}_{70}\text{EO}_{20}$  (Pluronic P123), as the surfactant and tetraethylorthosilicate (TEOS, analytical reagent) as the silica source, and the detailed synthesis procedure of SBA-15 can be found elsewhere [21]. The calcined SBA-15 was impregnated with aqueous solution of sucrose-containing sulfuric acid, similar to the synthesis of CMK-1 except for the different amounts of the sulfuric acid and sucrose. In brief, SBA-15 (1 g) was added to a solution obtained by dissolving sucrose (1.25 g) and  $\text{H}_2\text{SO}_4$  (0.14 g) in distilled  $\text{H}_2\text{O}$  (5 g). The mixture was placed in a drying oven for 6 h at 100 °C, and subsequently the oven temperature was increased to 160 °C and maintained there for 6 h. The sample turned to dark brown or black during the treatment in the oven. The silica sample containing partially polymerized and carbonized sucrose at the present step, was treated again at 100 and 160 °C using the same drying oven after addition of sucrose (0.8 g),  $\text{H}_2\text{SO}_4$  (0.09 g), and  $\text{H}_2\text{O}$  (5 g). The carbonization was completed by pyrolysis through heating to typically 900 °C under  $\text{N}_2$  atmosphere. The carbon–silica composite was obtained. The silica template was removed by hydrofluoric acid (HF) at room

temperature. The carbon product thus obtained was filtered, washed with deionized water and ethanol, and dried.

The composites were prepared by a combination of incipient wetness impregnation and hydrothermal method. Afterward, the synthesis of composite is as follows:  $\text{Ni}(\text{NO}_3)_2 \cdot 6\text{H}_2\text{O}$  (0.8296 g) and 50%  $\text{Mn}(\text{NO}_3)_2 \cdot 6\text{H}_2\text{O}$  (1.6379 g) (molar ratio = 1:1) were dissolved in 2.5 mL distilled water. Then OMC (0.5 g) was added to the above solution, stirred for 60 min, and heated at 250 °C for 2 h in autoclave to obtain OMC/binary Ni–Mn compound composite (OMCMN). According to different guest element, it was defined as OMCN, OMCM, and OMCMN, where N indicates the nickel compounds and M represents the manganese compounds. 50%  $\text{Mn}(\text{NO}_3)_2 \cdot 6\text{H}_2\text{O}$  and  $\text{Ni}(\text{NO}_3)_2 \cdot 6\text{H}_2\text{O}$  loading amounts of OMCM, OMCN, and OMCMN are listed in Table 1. The electrode of OMCMN was prepared according to the following steps. The mixture containing 75 wt% OMCMN, 20 wt% BP2000, and 5 wt% polytetrafluoroethylene (PTFE) was well mixed and then was pressed onto nickel foam (10 MPa) that serves as a current collector, and then dried at 90 °C for 1 h. The mass of activated substance in each electrode ranged from 4 to 5 mg. The electrochemical behavior of OMCMN was characterized by cyclic voltammetry (CV) tests. The electrochemical performance of the composites was analyzed using a three-electrode configuration in aqueous 2.0 M KOH electrolyte. The prepared OMCMN electrode was used as the working electrode, a saturated calomel electrode (SCE) was used as the reference electrode, and a platinum foil of convenient area was set as the counter electrode.

Cyclic voltammetry was performed on a CHI600C electrochemical workstation in the potential range of −0.1 to 0.5 V (vs. Ag/AgCl) with scan rates from 5 to 50 mV s<sup>−1</sup>. The specific capacitance at a given scan rate  $v$ , was calculated from voltammetric response using the following equation [22]:

$$C_s = \frac{1}{mv(V_f - V_i)} \int_{V_i}^{V_f} I(V)dV \quad (1)$$

where  $C_s$  is the specific capacitance of the capacitor ( $\text{F g}^{-1}$ ),  $m$  is the mass of the activated substance,  $V_f$  and  $V_i$  are the two integration limits of the voltammetric curve,

**Table 1** 50%  $\text{Mn}(\text{NO}_3)_2 \cdot 6\text{H}_2\text{O}$  and  $\text{Ni}(\text{NO}_3)_2 \cdot 6\text{H}_2\text{O}$  loading amount of OMCM, OMCN and OMCMN

Samples	50% $\text{Mn}(\text{NO}_3)_2 \cdot 6\text{H}_2\text{O}$ (g)	$\text{Ni}(\text{NO}_3)_2 \cdot 6\text{H}_2\text{O}$ (g)
OMCM	3.2758	0
OMCN	0	1.6592
OMCMN	1.6379	0.8296

and  $I(V)$  is the voltammetric current. All electrochemical measurements were carried out at room temperature.

## 2.2 Structural characterization

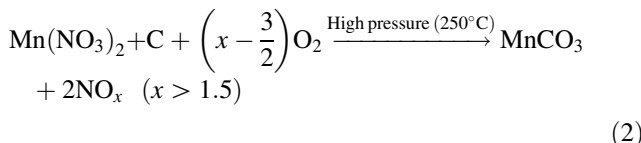
X-ray diffractions (XRD) of the samples were performed on a diffractometer (D/Max-rB II) with Cu K $\alpha$  radiation ( $\lambda = 1.54056 \text{ \AA}$ ) and a graphite monochromator at 50 kV, 100 mA.

Transmission electron micrographs (TEM) were taken on a JEOL-2010 microscope at an accelerating voltage of 200 kV.

Nitrogen physisorption measurements were recorded with an Autosorb 6 instrument (Quantachrome) at 77 K. Before the physisorption measurements the samples were outgassed at 423 K for 16–29 h. The surface areas were calculated from the adsorption branch in a region of  $p/p_0$  ranging from 0.03 to 0.20 applying the Brunauer, Emmet and Teller (BET) method. The pore size distributions were calculated using the desorption branch and applying the Barrett–Joyner–Halenda (BJH) method. The total pore volume was extracted from the adsorption branch using a respective data point with  $p/p_0$  in the range of 0.97–0.99.

## 3 Results and discussions

The X-ray diffraction patterns recorded for these composites after being heated at 250 °C in an autoclave while whose structural transformations taking place are shown in Fig. 1. The pattern of OMCN agrees with the position of the diffraction peaks of Ni(OH)<sub>2</sub> [JCPDS 14-0117] as a major phase and Ni<sub>3</sub>(NO<sub>3</sub>)<sub>2</sub>(OH)<sub>4</sub> [JCPDS 22-0752] as a minor phase. The surface modification of the peaks for the two compositions OMCN and OMCM reveals that they are uniformly embedded, while the OMCNM sample was poorly crystallized with a broad peak. It is noted that one new substance MnCO<sub>3</sub> [JCPDS 44-1472] appeared. The reason is possibly that the carbon framework supplies the carbon source. From a comparison of curves OMCM and Fig. 1b, the different diffraction peaks indicate what we assumed is possibly true under temperature of 250 °C. It is confirmed that others as the host material could not be obtained the MnCO<sub>3</sub>, such as SBA-15 shown in Fig. 1b. The possible reaction for that is



In the XRD pattern of the sample OMCNM, some distinct peaks indexed to Ni<sub>2</sub>(NO<sub>3</sub>)<sub>2</sub>(OH)<sub>2</sub>·2H<sub>2</sub>O [JCPDS 27-0952], Ni(OH)<sub>2</sub>, Mn<sub>3</sub>O<sub>4</sub> [JCPDS 24-0734], and MnCO<sub>3</sub> are clearly

shown. This suggests that the physical blending of the powders is well established. The sample OMCNM exhibits two peaks at  $2\theta = 11^\circ$  and  $22^\circ$ , which correspond to the (200) and (400) planes of Ni<sub>2</sub>(NO<sub>3</sub>)<sub>2</sub>(OH)<sub>2</sub>·2H<sub>2</sub>O, respectively. In addition, the peaks of (200) and (400) (indicated by □ in the Fig. 1) in OMCNM did not appear in OMCN, but appeared with weak intensities in the OMCNM samples. A comparison of the peaks of OMCN, OMCM, and OMCNM shows that most peaks corresponding to each plane of the composite shift slightly. It can be seen from the pattern of the sample OMCN and OMCM that the peak profile with relatively strong intensity and narrow line indicates good crystallinity.

N<sub>2</sub> sorption measurement shows that BET surface areas are 745 and 392 m<sup>2</sup> g<sup>-1</sup> for the OMC and the OMCNM, respectively. Figure 2 shows the N<sub>2</sub> adsorption–desorption isotherms of OMCNM and OMC. Although only OMC presents individually type IV isotherms according to the IUPAC classification, the volume adsorbed of N<sub>2</sub> decreases with nickel and manganese compounds loading amount. The pore characteristics, viz. BET surface area, total pore volume, and mean pore diameter determined by the N<sub>2</sub> adsorption–desorption isotherms are shown in Table 2. The parameters of porous texture are also found to have decreased with the metal compound loading amount, which resulted from the higher degree of pore filling. As shown in Fig. 2, the profile of the hysteresis loop indicates an adsorption–desorption characteristic of the porous materials. The pore size distribution shown in Fig. 2 as an insert suggests that the ordered mesostructured composition has a narrow pore size distribution centered at about 4 nm.

The pore and particle distribution and morphologies of OMC and OMCNM were examined by a transmission electron microscope (TEM) and typical results are shown in Fig. 3. The TEM image showed in Fig. 3a confirms that OMC with high degree of ordered porous texture is obtained from the carbon source of sucrose. It seems that the surface of the pores has been loaded with some products, which are testified as Mn<sub>3</sub>O<sub>4</sub>, Ni<sub>2</sub>(NO<sub>3</sub>)<sub>2</sub>(OH)<sub>2</sub>·2H<sub>2</sub>O, Ni<sub>3</sub>(NO<sub>3</sub>)<sub>2</sub>(OH)<sub>4</sub>, MnCO<sub>3</sub>, and Ni(OH)<sub>2</sub> in the XRD analysis (Fig. 1). Most sections have been covered very well as we can see from the above images (Fig. 3).

For quantitatively comparing the capacitance performances of different electrodes, the specific capacitance values are measured based on the cyclic voltammetric (CV) results, according to the Eq. (1). It can be concluded that the specific capacitances of the OMCNM composite are superior to those of the others in each corresponding cases and the maximum increment is approximately 2.5 times (435 vs. 196 F g<sup>-1</sup>) in 2 M KOH electrolyte. Moreover, it is noticed that the composite electrode exhibits higher specific capacitances than others at various scan rates except OMCM at 50 mV s<sup>-1</sup>. The pseudocapacitance

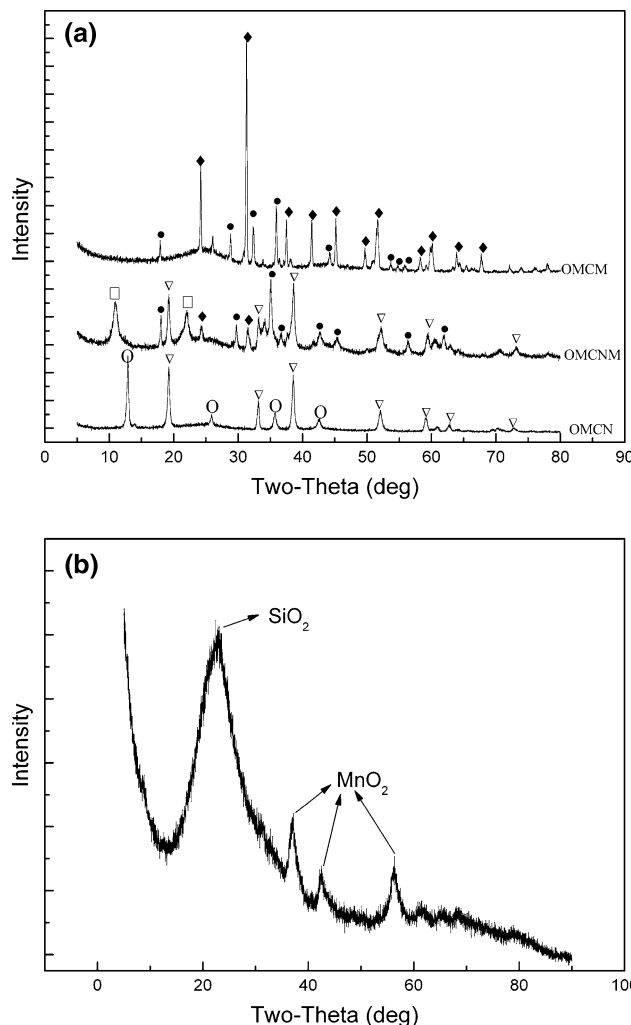
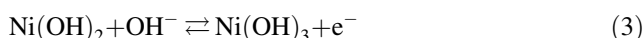


**Fig. 1** XRD patterns of OMCN, OMCNM, OMCM (a); and SBA-15/MnO<sub>2</sub> composite (b) position of the peaks expected for the (●) Mn<sub>3</sub>O<sub>4</sub>, (□) Ni<sub>2</sub>(NO<sub>3</sub>)<sub>2</sub>(OH)<sub>2</sub>·2H<sub>2</sub>O, (○) Ni<sub>3</sub>(NO<sub>3</sub>)<sub>2</sub>(OH)<sub>4</sub>, and (◆) MnCO<sub>3</sub>, (▽) Ni(OH)<sub>2</sub>

reaction of OMCNM electrode is expected to include the conversions of the redox couples in applied potential range, such as Mn(IV)/Mn(II) and Ni (III)/Ni(II). Therefore, it can be seen that the two pairs of redox peaks become somewhat unclear, demonstrating the well filling of binary Mn–Ni oxides in the pore of OMC and the host–guest structure. According to Yuan et al. [23], The electrochemical process can be presented as follows:



The two reactions of the electrochemical process could be screened in Fig. 5, which presented two pairs of redox peaks at the high scan rate.

To further specify the properties of OMCNM, the effects of potential scan rates (5–50 mV s<sup>-1</sup>) on the CV behavior

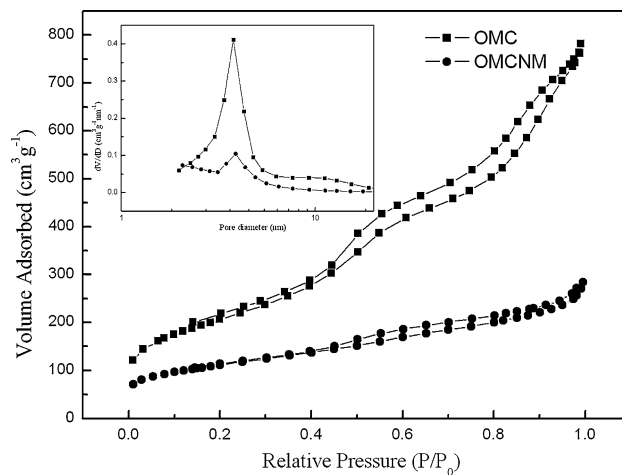


**Fig. 2** N<sub>2</sub> adsorption/desorption isotherms and pore size distributions (the inset) of OMC and OMCNM

**Table 2** Pore characteristics of OMC and OMCNM

Sample	S <sub>BET</sub> (m <sup>2</sup> g <sup>-1</sup> )	V <sub>t</sub> (cm <sup>3</sup> g <sup>-1</sup> )	Mean pore size (nm)
OMC	745	1.14	5.57
OMCNM	392	0.44	5.06

were investigated. Figure 5 presents the CV curves of OMCNM at various scan rates of 5, 10, 20, 30, and 50 mV s<sup>-1</sup>. Obviously, with the speed-up of the potential scan rate, the specific capacitances of electrodes are decreased markedly. For instance, the specific capacitance of the OMCNM composite electrode decreases to 187 F g<sup>-1</sup> at the scan rate of 50 mV s<sup>-1</sup> in 2 M KOH electrolyte, which is 43.1% of that measured at 5 mV s<sup>-1</sup>. That the performance of OMCNM is much better than others is closely related to the synergistic effect in this system. The ideal behavior indicates that the redox process occurs continuously. Since these processes are reversible, the charge storage in binary oxide is facilitated to yield pseudocapacitance behaviour. It implies that synergistic effects between nickel and manganese ions during the electrochemical process significantly changed the charge/discharge mechanism in a way leading to a much improved reversibility of the electrochemical reactions undertaken by OMC and OMCN electrodes. This good performance is attributed to the good ionic as well as electronic conductivity and low fluid diffusional limitations offered by the mesoporous support as reported by Samant et al. [24].

Though this combination exhibits the highest value, the capacitance values observed for the individual components as against their mutual combination are also interesting. The composite OMCNM is found to produce the highest specific capacitance except the highest scan rate. The presence of Ni<sub>2</sub>(NO<sub>3</sub>)<sub>2</sub>(OH)<sub>2</sub>·2H<sub>2</sub>O increases the electronic properties of the manganese compounds and improves the

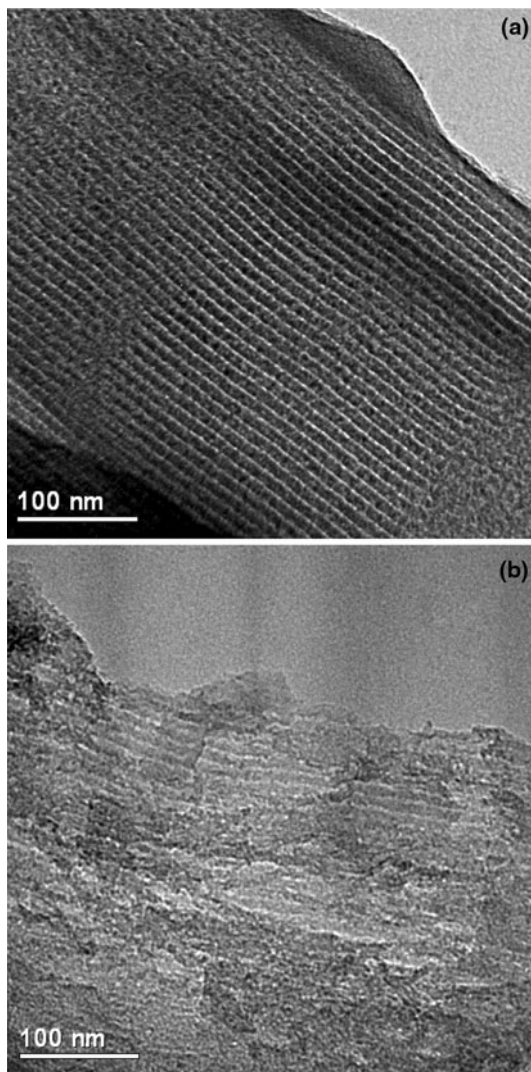


**Fig. 3** TEM images of **a** the ordered mesoporous carbon (OMC) and **b** OMCNM

capacitive behavior. An enhancement in the electrochemical active surface area of binary Mn–Ni compounds was found much more when nickel and manganese compounds were mixed under the atomic scale [25], which can be confirmed by XRD analysis. We have mentioned that one new substance  $\text{MnCO}_3$  appeared from the source of carbon framework and nitrate manganese. At the highest scan rate, it presented the highest value of specific capacitance, which is more or less equal to the OMCNM (Fig. 6).

The typical results are shown in Fig. 7. Two distinct regions which are dependent on the frequency range are shown in Fig. 7. From the point intersecting with the real axis in the range of high frequency (shown as an insert), the internal resistances  $R_i$  of both the electrodes are about  $0.5\Omega$ . It includes the total resistances of the electrode resistance,  $R$  electrode, the bulk electrolyte resistance,  $R_{\text{bulk}}$ , and the resistance at electrolyte/electrode interface,

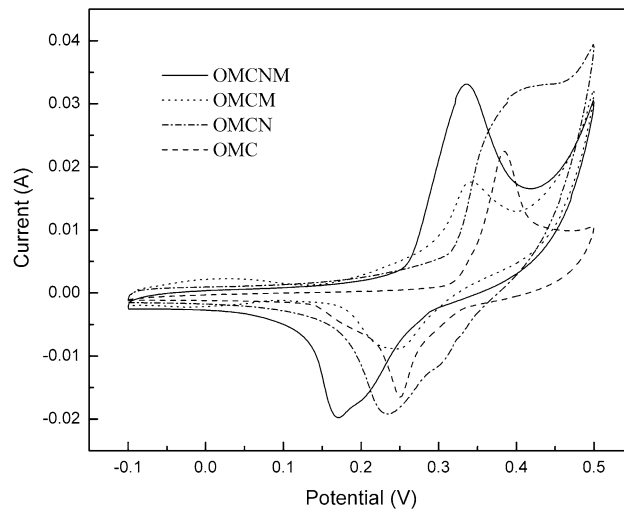


**Fig. 4** Cyclic voltammograms of pristine OMC, OMCNM, OMCM, and OMCN composites electrodes, measured in 2 M KOH solution with the potential scan rate of  $5 \text{ mV s}^{-1}$

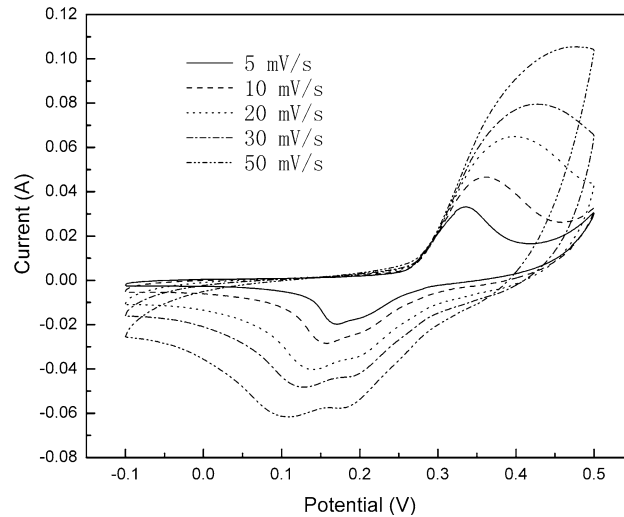


**Fig. 5** Cyclic voltammograms of OMCNM at various scan rates

$R$  interface. The phase angles for the impedance plots of both the electrodes of OMC and OMCM were observed to be higher than  $45^\circ$  in the high frequencies clearly. These findings suggest that both the electrodes are not controlled by diffusion process according to Cao et al. [26], whereas OMNM and OMCN electrodes were controlled by the diffusion process. The theory reported by Cao et al. agrees well with this study. Pristine OMC possessed the bigger pores without any loading amount of metal compounds and not controlled by the diffusive resistivity of the electrolyte within the pores of the electrode. The carbon sources of  $\text{MnCO}_3$  led to the collapse of OMC framework, which resulted of the increase of the pore diameter. It is quite different from the results reported by Wang and Xia [27].

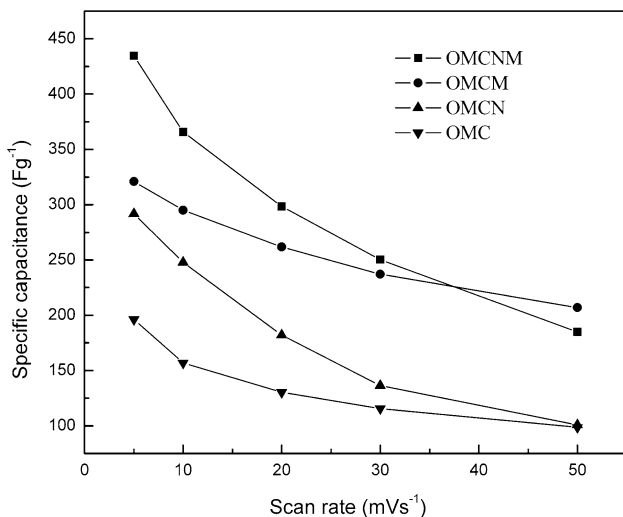


**Fig. 6** Specific capacitance of pristine OMC, Ni–Mn binary compounds/OMC, MnO<sub>2</sub>/OMC and Ni(OH)<sub>2</sub>/OMC as function of scan rate

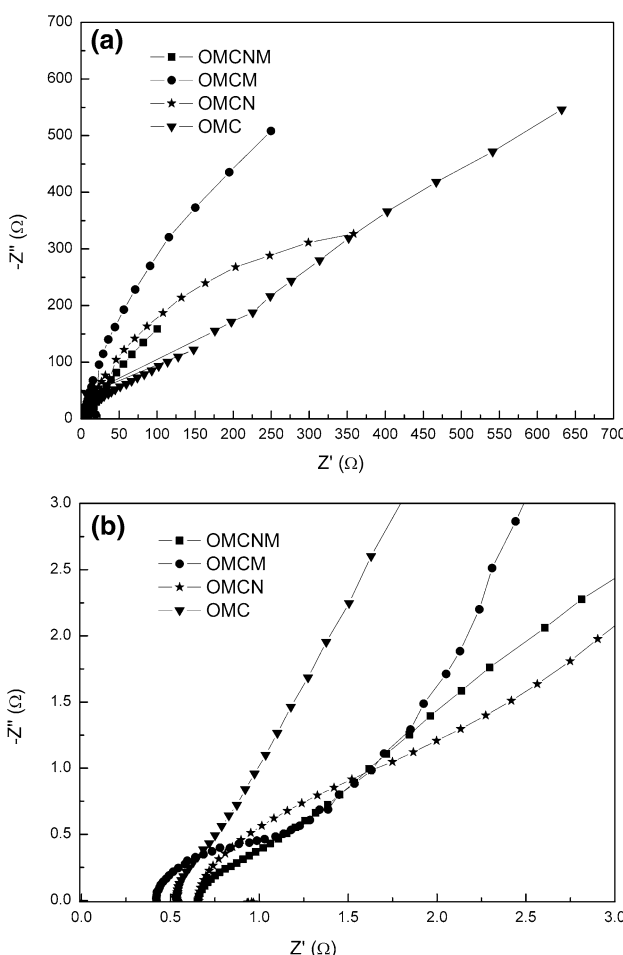


**Fig. 7** Typical electrochemical impedance spectroscopy of OMCNM, OMCM, OMCN, and OMC (a); enlargement of the high frequency part (b)

#### 4 Conclusions

The OMCNM nanocomposite, which had a synergistic effect of the complementary properties of both components, was obtained by a combination of incipient wetness impregnation and hydrothermal method not reported hitherto. Electrochemical tests indicated that this composite had a high specific capacitance (434 F g<sup>-1</sup>). The specific capacitance of the composite was about 2.5 times as compared with pure OMC. Furthermore, from the XRD analysis, we could conclude the framework of OMC can afford the carbon source to obtain MnCO<sub>3</sub> from 50% Mn(NO<sub>3</sub>)<sub>2</sub>·6H<sub>2</sub>O. Further study is, however, clearly warranted to understand the dynamic electrochemical and structural changes occurring during hydrothermal treatment and the process of charge–discharge.

**Acknowledgments** This study was financially supported by the Science and Technology Commission of Shanghai Municipality (no. 0952nm02500), and the Scientific Research Foundation of Graduate School of Shanghai University of Engineering Science (no. B8909080116).

#### References

- Jacob GM, Yang QM, Zhitomirsky L (2009) J Appl Electrochem 39:2579
- Faye A, Dione G, Dieng MM, Aaron JJ, Cachet H, Cachet C (2010) J Appl Electrochem 40:1925
- Kotz R, Carlen M (2000) Electrochim Acta 45:2483
- Burke A (2000) J Power Source 91:37
- Cui L, Li J, Zhang XG (2009) J Appl Electrochem 39:1871
- Lee JY, Liang K, An KH, Lee YH (2005) Synth Met 150:153
- Yan SC, Qu P, Wang HT, Tian T, Xiao ZD (2008) Mater Res Bull 43:2818
- He XJ, Geng YJ, Oke S, Higashi K, Yamamoto M, Takikawa H (2009) Synth Met 159:7
- Li HF, Wang RD, Cao R (2008) Microporous Mesoporous Mater 111:32
- Hu CC, Chang KH (2000) Electrochim Acta 45:2685
- Sugimoto W, Shibutani T, Murakami Y, Takasu Y (2002) Electrochim Solid State Lett 5:A170
- Lee BJ, Sivakkumar SR, Ko JM, Kim JH, Jo SM, Kim DY (2007) J Power Source 168:546
- Chen Y, Liu CG, Liu C, Lu GQ, Cheng HM (2007) Mater Res Bull 42:1935
- Li J, Zhitomirsky I (2009) J Mater Process Technol 209:3452
- Subramanian V, Zhu HW, Wei BQ (2006) Electrochim Commun 8:827
- Raymundo-Pinero E, Khomenko V, Frackowiak E, Beguin F (2005) J Electrochim Soc 152:A229
- Li J, Wang XY, Huang QH, Gamboa S, Sebastian PJ (2006) J Power Source 160:1501
- Kuo SL, Wu NL (2006) J Power Source 162:1437
- Zhu S, Zhou H, Hibino M, Honma I, Ichihara M (2005) Adv Funct Mater 15:381
- Feng JC, Zhao JC, Tang BHJ, Liu P, Xu JL (2010) J Solid State Chem 183:2932
- Zhao D, Feng J, Huo Q, Melosh N, Fredrickson GH, Chmelka BF, Stucky GD (1998) Science 279:548

22. Panic V, Vidakovic T, Gojkovic S, Dekanski A, Nikolic B (2003) *Electrochim Acta* 48:3805
23. Yuan CZ, Zhang XG, Wu QF, Gao B (2006) *Solid State Ion* 177:1237
24. Samant PV, Fernandes JB, Rangel CM, Figueiredo JL (2005) *Catal Today* 102–103:173
25. Trasatti S (1991) *Electrochim Acta* 36:225
26. Cao L, Lu M, Li HL (2005) *J Electrochem Soc* 152:A871
27. Wang YG, Xia YY (2006) *Electrochim Acta* 51:3223